

- Mol. Catal.* **62**, 277 (1990); J. J. W. Eshuis *et al.*, *Organometallics* **11**, 362 (1992); L. Resconi, F. Piemontesi, G. Francisconi, L. Abis, T. Fiorani, *J. Am. Chem. Soc.* **114**, 1025 (1992); J. Boor, *Ziegler-Natta Catalysts and Polymerizations* (Academic Press, New York, 1979).
16. PAXAS Programme for the Analysis of X-Ray Absorption Spectra; N. Binsted, University of Southampton, Southampton, UK (1988).
17. S. J. Gurman, N. Binsted, I. Ross, *J. Phys. C* **17**, 143 (1984); *ibid.* **19**, 1845 (1986).
18. J. M. Corker and J. Evans, *Chem. Commun.* **1994**, 1027 (1994).
19. R. W. Joyner, K. J. Martin, P. Meehan, *J. Phys. C* **20**, 4005 (1987).
20. F. W. Lytle, D. E. Sayers, E. A. Stern, *Physica B* **158**, 701 (1989).

8 August 1995; accepted 3 November 1995

## Lamellar Biogels: Fluid-Membrane-Based Hydrogels Containing Polymer Lipids

Heidi E. Warriner, Stefan H. J. Idziak, Nelle L. Slack, Patrick Davidson,\* Cyrus R. Safinya†

A class of lamellar biological hydrogels comprised of fluid membranes of lipids and surfactants with small amounts of low molecular weight poly(ethylene glycol)-derived polymer lipids (PEG-lipids) were studied by x-ray diffraction, polarized light microscopy, and rheometry. In contrast to isotropic hydrogels of polymer networks, these membrane-based birefringent liquid crystalline biogels, labeled  $L_{\alpha,g}$ , form the gel phase when water is added to the liquid-like lamellar  $L_{\alpha}$  phase, which reenters a liquid-like mixed phase upon further dilution. Furthermore, gels with larger water content require less PEG-lipid to remain stable. Although concentrated ( $\sim 50$  weight percent) mixtures of free PEG (molecular weight, 5000) and water do not gel, gelation does occur in mixtures containing as little as 0.5 weight percent PEG-lipid. A defining signature of the  $L_{\alpha,g}$  regime as it sets in from the fluid lamellar  $L_{\alpha}$  phase is the proliferation of layer-dislocation-type defects, which are stabilized by the segregation of PEG-lipids to the defect regions of high membrane curvature that connect the membranes.

Gels are viscoelastic materials that normally consist of a solid component dispersed in a liquid, water in the case of hydrogels. Polymer gels (1)—either natural, such as gelatin, or synthetic—contain a polymer network (2), which serves as the solid component and can resist shear. For many biological applications, gels based on high molecular weight poly(ethylene oxide) [PEO,  $(\text{OCH}_2\text{CH}_2)_n$ ] (3) have been used because of their low immunogenicity: the material can be used to coat more immunogenic tissues (1) and materials (4).

Recent studies show that attaching low molecular weight ( $n < 150$ ) PEO (referred to as PEG) to a biological macromolecule (5–8) can dramatically increase blood circulation times. Both peptides and proteins can be protected by covalently attached PEG for in vivo administration of therapeutic enzymes (5), and so-called “Stealth” liposomes (6–8) consisting of closed bilayer shells of phospholipids covered with PEG-lipids hydrophobically anchored to the membrane can be used as a drug carrier system. The inhibition of the body’s im-

mune response to these PEG-coated liposomes has been attributed (8) to a polymer-brush-type steric repulsion (9) that has been measured between PEG-coated membranes incorporated both in the chain-frozen membrane phase on a solid substrate (10) and in the chain-melted fluid phase in multilamellar  $L_{\alpha}$  systems (11). In these systems, the emphasis was in the regime where the intermembrane distance  $d \leq R_g$ , where  $R_g$  is the PEG radius of gyration.

In exploring the interactions between PEG-lipid and the chain-melted fluid phase in multilamellar  $L_{\alpha}$  systems, we have discovered a lamellar hydrogel phase, labeled  $L_{\alpha,g}$ , in the high water regime of the phase diagram. This gel incorporates no solid phase component. Polarized light microscopy has revealed that this phase is not isotropic and shows liquid crystal-like birefringence. Studies with x-ray diffraction show that the maximum interlayer spacings  $d \gg R_g$  for this phase (Fig. 1A); a model for the structure of this phase suggests that PEG-lipid stabilizes layer dislocation defects in regions of high membrane curvature (Fig. 1B). Unlike  $L_{\beta}$  gels that incorporate solid membranes (12), a bioactive gel based on fluid membranes could incorporate membrane-embedded proteins that are biologically active, thus providing a way in which to deliver such molecules in a stable gel. An unusual feature of these gels is that they can be formed from a liquid-like flowing  $L_{\alpha}$

phase by adding water and also dissolved back to a flowing two-phase liquid by further addition of water.

The  $L_{\alpha,g}$  phase is composed of membranes of DMPC (dimyristoyl phosphatidyl choline), the co-surfactant pentanol, and small amounts of the polymer-lipid PEG-DMPE {1,2-diacyl-*sn*-glycero-3-phosphoethanolamine-*N*-[poly(ethylene glycol)]} separated by water. The PEG-lipid is hydrophobically anchored but free to diffuse within the fluid membrane (Fig. 1A). We investigated two different molecular weights of PEG, 2053 g/mol (PEG2000;  $n = 45$  monomers) and 5181 g/mol (PEG5000;  $n = 113$ ) (Avanti Polar Lipids, Alabaster, Alabama). The most dilute gels contained 90.0 weight % water, 6.0 weight % lipid, 3.46 weight % pentanol, and 0.54 weight % PEG5000-DMPE (Fig. 2). In contrast, the conventional solid-membrane  $L_{\beta}$  gels incorporate at most 40 weight % water (12). In principle, addition of PEG-lipid to even more dilute  $L_{\alpha}$  phases [ $\approx 99$  weight % (13)] would result in extremely dilute lamellar gels.

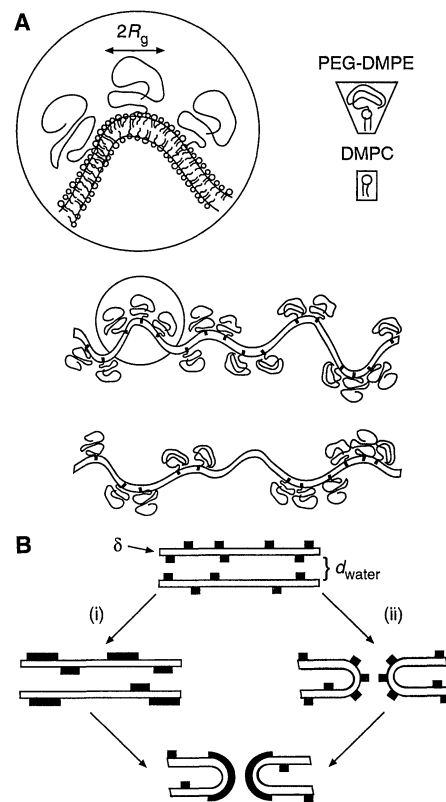


**Fig. 1.** (A) Schematic of two undulating fluid membranes [composed of DMPC and co-surfactant pentanol (single chain)] with PEG-lipid hydrophobically anchored but freely diffusing within the membrane. (B) Schematic of two paths that would form defects, with the laterally phase separated PEG-lipid residing in, and stabilizing, the regions of high curvature. The interlayer spacing is  $d = \delta + d_{\text{water}}$ , where  $\delta$  is the membrane thickness and  $d_{\text{water}}$  is the separation between layers containing water and the hydrophilic PEG component.

Materials Research Laboratory, Materials Department, Physics Department, and the Interdepartmental Biochemistry and Molecular Biology Program, University of California, Santa Barbara, CA 93106, USA.

\*Permanent address: Laboratoire de Physique des Solides (CNRS), Bat. 510, Université Paris Sud, 91405 Orsay, Cedex, France.

†To whom correspondence should be addressed.

For both molecular weights of PEG-DMPE, sample viscosity increases dramatically with the onset of gelation, occurring both as a function of increasing PEG-lipid concentration and, unexpectedly, as a function of increasing water concentration. Remarkably, we find an inverse behavior for gelation, with mixtures of larger water content gelling at lower PEG-lipid concentrations. An important finding is the formation of hydrogels containing as low as 0.5 weight % PEG-lipid, which is much smaller than a monolayer coverage of the bilayers. Polymer hydrogels consisting of free PEG at such low concentrations would require molecular weights of PEO of order a million.

The key difference with previous work (11) that allowed us to explore the regime  $d \gg R_g$ , where the biogel is stable, was the high flexibility of the fluid membranes within which the PEG-lipid was incorporated. Without PEG-lipid, the addition of the co-surfactant pentanol to membranes consisting of DMPC thins the bilayer membrane, which leads to the decrease of its bending rigidity  $\kappa \approx k_B T$  (thermal energy) (14). The lamellar  $L_\alpha$  phase is then comprised of fluid, highly flexible membranes with interactions dominated by long-range repulsive undulation forces (14–16), giving rise to large intermembrane distances. In our studies, we fixed the ratio of pentanol to lipid molecules at  $\sim 4:1$ , which corresponds to bilayers of thickness  $\delta = 28 \text{ \AA}$  (14).

In the case of PEG5000-DMPE, for water weight fraction  $\Phi_w < 0.66$ , which is below the lower two-phase boundary on the phase diagram (Fig. 2), the stacked bilayers cannot incorporate any PEG5000. This boundary corresponds to an average membrane separation  $d_{\text{water}} \approx 60 \text{ \AA}$ . For PEG2000-DMPE, the two-phase boundary occurs at  $d_{\text{water}} \approx 25 \text{ \AA}$ . Thus, as a function of increasing water, the one-phase lamellar region is stable when the separation distance is approximately large enough to accommodate the swollen PEG polymer. The maximum spacings where the

lamellar regions remain one-phase correspond to  $d_{\text{water}} = 390 \text{ \AA} \approx 6R_g$  for PEG5000-DMPE, and  $d_{\text{water}} = 286 \text{ \AA} \approx 8R_g$  for PEG2000-DMPE (Fig. 2, inset) [for PEG-lipid in lipid membranes,  $R_g$  has been measured to be about 35 and 62  $\text{\AA}$  for PEG2000 and PEG5000, respectively (10, 11)].

At water concentrations  $\Phi_w > 0.66$  and low PEG-lipid concentrations, we observe a low viscosity, lamellar liquid-crystal (LC)  $L_\alpha$  phase qualitatively similar in appearance to  $L_\alpha$  samples not incorporating PEG-lipid. However, mixtures changed from a flowing to a gelling lamellar phase upon the addition of either PEG-lipid or water (Fig. 2). Using approximate numbers for the PEG radii of gyration together with those for the areas of lipid and co-surfactant molecules (10, 11), we estimated the concentration where the mushroom-shaped PEG-lipid first covers a flat membrane before any overlap of the polymer chains occurs to be about 3 mol% for PEG5000-DMPE and 8 mol% for PEG2000-DMPE. The transition to the gel phase then occurs in PEG-lipid concentrations below the brush regime, where the polymer does not fully coat the membrane. Thus, the direct interactions between the PEG on opposing layers can be ruled out as a mechanism for gelation. In addition, the gel samples can be prepared in brine (for example, 0.5 M NaCl), which rules out long-range electrostatic interactions (17) in gel formation (18).

We placed four mixtures of varying  $\Phi_w$  [spanning three regions of the phase diagram (Fig. 2)] in glass tubes tilted to allow flow (Fig. 3A). As  $\Phi_w$  increased initially from 0.45 to 0.68, the sample flowed more easily, which is the typical expected behavior observed in complex fluids as a function of solvent dilution (13). Upon further increase in the water fraction, the sample gelled at  $\Phi_w \approx 0.71$ ; elasticity dominated, and the mixture, which abruptly ceased to flow, had properties of a weak solid. Mixtures of free PEG (molecular weight, 2000)

and water do not gel, even when extremely concentrated (for example, as large as 90 weight % PEG). As we added more water, the mixture dissolved into a liquid-like two-phase region (Fig. 3A, top tube). The  $L_{\alpha,g}$  phase is a physical gel rather than a traditional chemical gel, which has permanent covalent-bond cross-links (2).

The gel samples can sustain arbitrary shapes against surface tension and gravity for indefinite periods. The nonspherical stable bubbles (Fig. 3B) show that the sample has a yield stress resisting surface tension forces, as expected for a gel. The real (storage elasticity modulus  $G'$ ) and imaginary

**Fig. 2.** Phase diagram for PEG5000-DMPE (solid line) and PEG2000-DMPE (dashed line), plotted in terms of the water weight fraction  $\Phi_w$  versus the concentration of PEG-lipid in the total lipid, denoted by  $c_{\text{PEG}}$  [ $100 \times$  (number of PEG-lipid molecules)/(total number of lipid molecules), where total lipid is DMPC + DMPE]. The lipid-to-pentanol weight ratio was  $2.0 \pm 0.25$ . Note that the gel regime is accessed by increasing either the PEG-lipid concentration or the water concentration. (Inset) Comparison of the fluid-gel transition lines for PEG5000-DMPE and PEG2000-DMPE, plotted with the interlayer spacing  $d = d_{\text{water}} + \delta$  instead of  $\Phi_w$ .

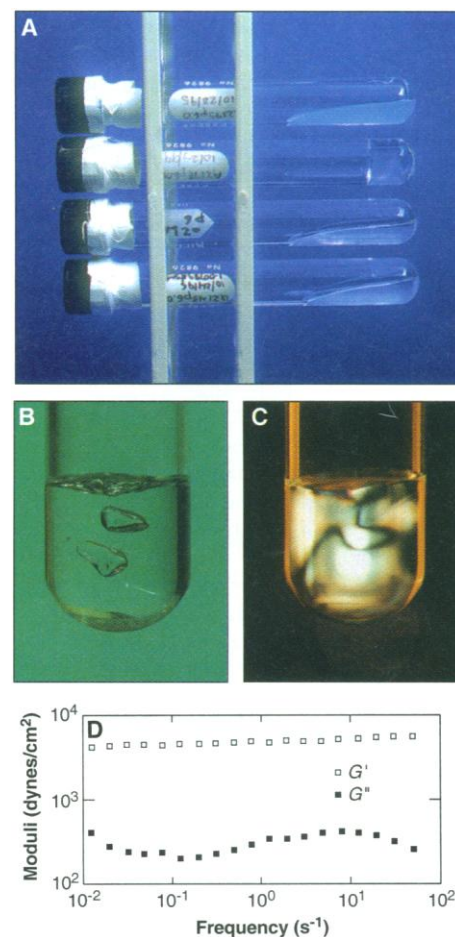
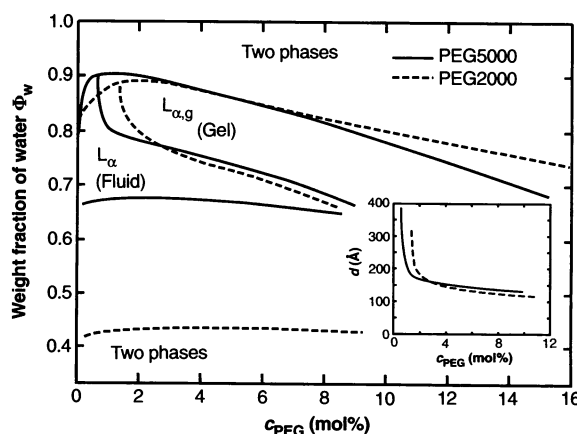


**Fig. 3.** (A) Four samples, each with a PEG2000-DMPE concentration of 6.06 mol% but increasing water content. From bottom to top:  $\Phi_w = 0.45$  (lamellar interlayer spacings  $d = 55 \text{ \AA}$ ,  $L_\alpha$  fluid), 0.68 ( $d = 110 \text{ \AA}$ ,  $L_\alpha$  fluid), 0.78 ( $d = 165.4 \text{ \AA}$ ,  $L_{\alpha,g}$  gel), and 0.95 (two-phase liquid-like). The test tubes are 13 mm in diameter. (B) Gel sample showing non-spherical bubbles. Bubbles like these have lasted more than 6 months. (C) The same gel sample viewed between crossed polarizers, showing liquid crystalline defects. (D) Dynamic elastic moduli for the  $\Phi_w = 0.78$  gel sample as a function of frequency (measured with a cone and plate rheometer). These data are typical of the gel samples in that the elastic storage modulus  $G'$  is substantially greater than the viscous loss modulus  $G''$  over the four decades of frequency measured.

(loss modulus  $G'' \propto$  viscosity) parts of the dynamic moduli were measured (19). As a function of increasing PEG2000-DMPE concentration,  $G'/G''$  varied between 4 and 20 in the gel phase (Fig. 3D).

The LC nature of the  $L_{\alpha,g}$  biogels distinguishes them from most natural- and biopolymer-based hydrogels (1, 2). When viewed between crossed polarizers (Fig. 3C), the samples are birefringent and LC defects (20) are visible on a millimeter scale.

Small-angle x-ray powder scans (21),

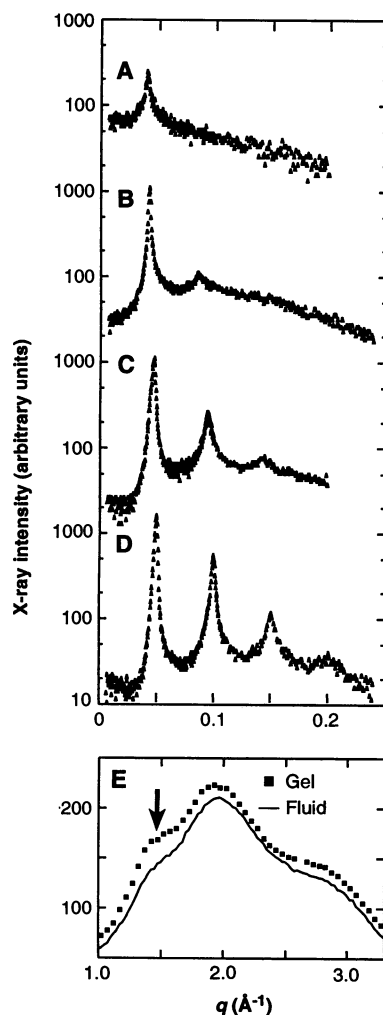


**Fig. 4.** (A through D) Synchrotron x-ray scattering data on four samples along an increasing PEG2000-DMPE line: (A)  $c_{\text{PEG}} = 0$  mol%,  $\Phi_w = 0.80$ ,  $d = 155$   $\text{\AA}$ ; (B)  $c_{\text{PEG}} = 2.9$  mol%,  $\Phi_w = 0.78$ ,  $d = 147$   $\text{\AA}$ ; (C)  $c_{\text{PEG}} = 7.8$  mol%,  $\Phi_w = 0.75$ ,  $d = 133$   $\text{\AA}$ ; (D)  $c_{\text{PEG}} = 15.5$  mol%,  $\Phi_w = 0.70$ ,  $d = 127$   $\text{\AA}$ . The first two samples are in the  $L_\alpha$  fluid, and the last two are in the  $L_{\alpha,g}$  gel regime, which sets in around  $c_{\text{PEG}} = 4.0 \pm 0.25$  mol% and  $\Phi_w = 0.76 \pm 0.02$  along this line. The emergence of harmonics with added polymer-lipid indicates an increase in the intermembrane repulsion. (E) In-plane scan for the  $c_{\text{PEG}} = 0$  mol% (fluid) and 7.8 mol% (gel) samples, showing the liquid-like chain interference peak at  $q = 1.5$   $\text{\AA}^{-1}$  (arrow) and the two water peaks at 2 and 2.7  $\text{\AA}^{-1}$ .

corresponding to the (001) peaks of the lamellar structure, are shown for four mixtures along a line of increasing PEG2000-DMPE concentration in the fluid (Fig. 4, A and B) and gel (Fig. 4, C and D) regions. The data shown are in mixtures where the total weight fraction of the hydrophilic portion of the multilayer phase, consisting of water and the water-soluble part of PEG-lipid ( $\Phi_w + \Phi_{\text{PEG}}$ ), was kept constant at 0.8 (with  $\Phi_w$  varying between 0.8 and 0.7) as  $c_{\text{PEG}}$  (mole concentration of PEG-lipid) was increased. This observed behavior, where the addition of PEG-lipid correlates with the emergence of higher harmonics in the scattering profile, is typical for both PEG2000-DMPE and PEG5000-DMPE (22). In a fluid lamellar phase (that is, both  $L_\alpha$  and  $L_{\alpha,g}$ ), the onset of the higher harmonics is an indication of the stiffening of the bulk compression modulus  $B$  (14, 16, 20). This suggests that PEG-coated membranes in a flexible multilayer system experience an enhanced repulsive interaction (23) as a function of increasing  $c_{\text{PEG}}$ , which is consistent with the measured increase in  $B$  (22).

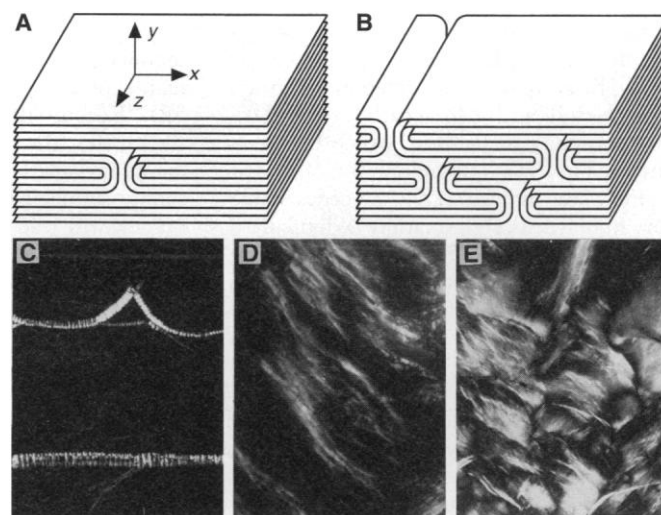
The value of  $B$  increases smoothly as  $c_{\text{PEG}}$  increases and the gel forms. The onset of the harmonics depends on  $c_{\text{PEG}}$  but is essentially independent of the water content  $\Phi_w$  (or  $d$ ); that is, harmonics do not emerge as dilution with water forms the gel. Thus, the increase in  $B$  is not directly related to the gel transition. Experiments at higher angles (Fig. 4E) verify that the interference peak at  $q = 1.5$   $\text{\AA}^{-1}$  caused by interactions between the lipid chains remains liquid-like in both the  $L_\alpha$  and  $L_{\alpha,g}$  regimes; thus, the addition of PEG-lipid

does not affect bilayer fluidity. Unlike  $L_\beta$  gels, gelation is not a result of in-plane chain ordering (12).

The onset of gelation is marked by a distinct change in the defect structure observed in polarized light microscopy (24). Samples in the fluid  $L_\alpha$  regime primarily exhibit homeotropic (lamellae parallel to the glass surfaces) alignment broken by the typical "oily streak" defects characteristic of lamellar phases with melted chains (Fig. 5C;  $xz$  plane). The basic form of the oily streak has been described previously in terms of a disclination-pair defect (Fig. 5A), each part of strength  $+1/2$  (25). Striations along the length of the defect ( $z$  axis) can be attributed to undulations of the defect axis in and out of alignment with the axes of the crossed polarizers (25). The defect structure can also be described in terms of two opposite edge dislocations with large Burgers vectors (20, 25).

As the transition to the  $L_{\alpha,g}$  region is approached, we observe a proliferation of these line defects, which are now significantly thinner (Fig. 5D). A cut through the sample exposing the  $xy$  plane normal to the line defects running along the  $z$  axis (Fig. 5B) would have a dense packing of edge-dislocation pairs. The closure of an edge-dislocation pair would produce a defect loop. The ends of the loop would consist of multilayers with layer normal along  $z$ , parallel to the defect lines. Within this "whispy" texture, which is a common textural observation in the  $L_{\alpha,g}$  phase, regions of densely packed and highly aligned line defects (Fig. 5E) provide evidence of what appears to be a nematic ordering of line

**Fig. 5.** Real space structure of defects in the (A) fluid  $L_\alpha$  and (B) gel  $L_{\alpha,g}$  phases. For simplicity, we show in (A) a defect pair with opposite Burgers vectors each of strength 6. Unequal Burgers vectors are expected with nonuniform sample thickness. In the  $L_\alpha$  phase, the defects can be annealed, whereas in the  $L_{\alpha,g}$  phase, the defects cannot be annealed. (C through E) Optical microscopy pictures of defects in PEG2000-DMPE samples along a line of increasing PEG-lipid concentration (with  $\Phi_w + \Phi_{\text{PEG}} \approx 0.8$ ). All photographs are of samples in 0.2-mm-thick flat rectangular glass capillaries observed between crossed polarizers. (C) Sample with  $c_{\text{PEG}} = 1.1$  mol% and  $\Phi_w = 0.79$  showing the oily streak defects typical of  $L_\alpha$  phases. (D) Mixture with  $c_{\text{PEG}} = 4.53$  mol% and  $\Phi_w = 0.78$  in the gel phase (gel transition at  $c_{\text{PEG}} = 4.0 \pm 0.25$  mol% and  $\Phi_w = 0.76 \pm 0.05$  along this line). The proliferation of the line defects is evident. (E) Defects in a sample with  $c_{\text{PEG}} = 4.2$  mol% and  $\Phi_w = 0.77$  in the gel phase, which in addition to the line defects also shows dark brushes attributable to disclinations of the defect lines.



defects in macroscopically large regions of the sample (26). On millimeter length scales, nematic-like (20) Schlieren defects are apparent (Figs. 3C and 5E); that is, nematic disclination defects of the (edge-dislocation) line defects. In contrast to the  $L_\alpha$  phase mixtures, in which the defects may be annealed, the densely packed defected  $L_{\alpha,g}$  texture cannot be annealed and is inherent to the gel phase.

A simple model of the lamellar fluid-gel transition is described by the softening of the free energy of line defects and their consequent proliferation as observed experimentally. This model is qualitatively consistent with the phase behavior, where gelation in mixtures with larger interlayer spacing (larger water content) occurs at smaller PEG-lipid concentrations. For simplicity, we consider the elastic cost of the simplest defect line consisting of an edge-dislocation pair of opposite Burgers vector of strength  $2$  (Fig. 1B, bottom). The membranes consist primarily of two components. The bare membrane component (DMPC and pentanol) has a natural radius of curvature  $C_0^P = 0$  (Fig. 1A, top right); that is, fluid membranes with this mixture are known to form stable lamellar  $L_\alpha$  phases (13, 16). The PEG-lipid component has a finite natural radius of curvature  $C_0^P > 0$  (Fig. 1A, top right) and is known to stabilize vesicles (7, 8, 11). At low PEG-lipid concentrations, the two components are uniformly mixed (Fig. 1B, top). As the PEG-lipid concentration increases, a frustration is built where the different components compete for varying membrane curvature. The formation of stable edge-dislocation defect lines observed experimentally satisfies both components where the regions of high curvature membrane are the aggregation sites of the PEG-lipid component (Fig. 1B, bottom). Two different pathways could be followed. Along path (i) (Fig. 1B), in-plane phase separation, which has been observed in PEG-lipid monolayers spread at an air-water interface (27), precedes stable curvature (defect) formation. Along path (ii), the coupling between the membrane curvature and concentration components may lead to a curvature-induced in-plane phase separation that would also result in stable defects consistent with recent theoretical work (28).

The elastic cost of forming a line defect of length  $L$  with edge curvature  $C = 2/d$  (that is, the two half cylinders shown in Fig. 1B, bottom) is given by the Helfrich elastic energy of fluid membranes (15)  $E_d = 0.5\pi\kappa Ld(C - C_0)^2$ , where  $C_0 = \Phi_v^{\text{PEG}} C_0^P$ ,  $\Phi_v^{\text{PEG}}$  is the volume fraction of PEG-lipid in the membrane, and  $\kappa$  is the membrane bending rigidity. The entropy gained in forming the line defect is given by  $TS = k_B TL/\xi_p$ , where  $\xi_p = \pi d\kappa/k_B T$  is the persistence length (29) of the

cylindrical membrane. The softening of the line free energy  $E_d - TS = 0$  then leads to the simple relation for the proliferation of line defects at the lamellar fluid-gel transition

$$d_{\text{gel}} = \frac{2 - 2^{1/2} k_B T / \pi \kappa}{\Phi_v^{\text{PEG}} C_0^P} \quad (1)$$

Because  $\Phi_v^{\text{PEG}}$  roughly scales as  $C_{\text{PEG}} V_{\text{PEG}}$ , where  $V_{\text{PEG}} = N v_{\text{PEG}}$  ( $N$  = degree of polymerization,  $v_{\text{PEG}}$  = volume of a monomer), Eq. 1 is qualitatively consistent with our experimental phase diagram, where  $d \propto 1/c_{\text{PEG}}(\text{gel})$  (Fig. 2, inset). This simple model not only contains the inverse relation between water and polymer content required for gelation but also gives the correct qualitative trend in the scaling behavior of the PEG2000-DMPE and PEG5000-DMPE systems. The natural radius of curvature  $C_0^P$  can be estimated from the result for an asymmetric block copolymer at a spherical vesicle interface calculated previously with  $C_0^P \propto 1/N^{2/3}$  (30). The scaling dependence of the interlayer spacing at the gel transition then behaves as  $d_{\text{gel}} \propto 1/\Phi_v^{\text{PEG}} C_0^P \propto 1/N^{1/3}$ . This result is qualitatively consistent with the phase diagram (Fig. 2, inset), where as we increase  $d$  at a constant PEG-lipid concentration  $< 2$  mol%, PEG5000-DMPE gels before PEG2000-DMPE. The schematic in Fig. 1B (bottom) gives a simple description of the model: Larger water fractions lead to a larger spacing  $d$  and consequently a smaller curvature (joining opposing bilayers), which in turn, requires less PEG-lipid.

The gel phase is then characterized by a highly defected microstructure comprised of a network of connected membrane bilayers with the PEG-lipid segregated to the high curvature regions (Fig. 1B), which on a semimacroscopic length scale leads to domains of random layer orientation (Fig. 5B). Recent theoretical work (31) has shown that the random orientation of domains in lamellar block copolymers, structurally similar to lamellar phases of membranes, will lead to elasticity and thus gel-like behavior because domains that have their layer normals with a finite projection along the flow direction will resist shear, because of the energetically unfavorable tilting of layers.

Because the principal component of these fluid membrane-based hydrogels is lipid and surfactant, "bioactive gels" useful in tissue healing or drug delivery applications (4, 7, 8) may be envisioned that derive their activity from membrane-anchored peptides, proteins, or other drug molecules and their mechanical stability from the polymer-lipid minority component. Alternatively, in analogy to so-called "smart" hydrogels of polymer networks, which respond by contracting or expanding

to external stimuli such as temperature, solvent, or pH changes (1, 32), a suitable choice of lipid and polymer-lipid should lead to a different class of smart lamellar hydrogels.

## REFERENCES AND NOTES:

- See, for example, D. DeRossi, K. Kajiwara, Y. Osada, A. Yamauchi, Eds., *Polymer Gels: Fundamentals and Biomedical Applications* (Plenum, New York, 1991).
- In a polymer chemical gel, the network consists of covalent cross-links. In a polymer physical gel, the network is formed either through temporal entanglements or interactions (for example, electrostatic, van der Waals, hydrogen-bonding, or hydrophobic interactions) between macromolecular sections [see, for example, S. B. Ross-Murphy, in (1), p. 21].
- See, for example, F. E. Bailey Jr. and J. V. Koleske, Eds., *Poly(Ethylene Oxide)* (Academic Press, New York, 1976).
- N. A. Peppas and R. Langer, *Science* **263**, 1715 (1994).
- See, for example, V. H. L. Lee, Ed., *Peptide and Protein Drug Delivery* (Dekker, New York 1991); E. Marshall, *Science* **269**, 1050 (1995).
- T. M. Allen and A. Chonn, *FEBS Lett.* **223**, 42 (1987); A. Gabizon and D. Papahadjopoulos, *Proc. Natl. Acad. Sci. U.S.A.* **85**, 6949 (1988).
- D. D. Lasic, *Liposomes: From Physics to Applications* (Elsevier, Amsterdam, 1993).
- See, for example, D. D. Lasic and D. Papahadjopoulos, *Science* **267**, 1275 (1995); D. D. Lasic and F. J. Martin, Eds., *Stealth Liposomes* (CRC Press, Boca Raton, FL, 1995).
- S. Alexander, *J. Phys. France* **38**, 977 (1977); P.-G. De Gennes, *ibid.* **37**, 1443 (1976); *Macromolecules* **13**, 1069 (1980); S. T. Milner, *Science* **251**, 905 (1991).
- T. L. Kuhl, D. E. Leckband, D. D. Lasic, J. N. Israelachvili, *Biophys. J.* **66**, 1479 (1994).
- D. Needham, T. J. McIntosh, D. D. Lasic, *Biochim. Biophys. Acta* **1108**, 40 (1992); A. K. Kemworthy, K. Hristova, D. Needham, T. J. McIntosh, *Biophys. J.* **68**, 1921 (1995).
- A. Tardieu, V. Luzzati, F. C. Reman, *J. Mol. Biol.* **75**, 711 (1973); D. M. Small, in *The Physical Chemistry of Lipids*, vol. 4 of *Handbook of Lipid Research*, D. M. Small, Ed. (Plenum, New York, 1986); G. S. Smith, E. B. Sirota, C. R. Safinya, N. A. Clark, *Phys. Rev. Lett.* **60**, 813 (1988); G. S. Smith, E. B. Sirota, C. R. Safinya, R. J. Plano, N. A. Clark, *J. Chem. Phys.* **92**, 4519 (1990).
- See, for example, A. Ben-Shaul, W. M. Gelbart, D. Roux, Eds., *Micelles, Membranes, Microemulsions and Monolayers* (Springer-Verlag, New York, 1994).
- C. R. Safinya, E. B. Sirota, D. Roux, G. S. Smith, *Phys. Rev. Lett.* **62**, 1134 (1989).
- W. Helfrich, *Z. Naturforsch. A* **33**, 305 (1978); *Z. Naturforsch. C* **28**, 693 (1973).
- C. R. Safinya et al., *Phys. Rev. Lett.* **57**, 2718 (1986).
- Each PEG-lipid has one negative charge; however, the membrane charge density is very low because of the low PEG-lipid concentration.
- D. Roux and C. R. Safinya, *J. Phys. France* **49**, 307 (1988).
- Constant-stress oscillatory shear-strain experiments were carried out with a Rheometrics dynamic stress rheometer, model 1710C.
- P.-G. De Gennes and J. Prost, *The Physics of Liquid Crystals* (Clarendon, Oxford, ed. 2, 1993).
- High-resolution x-ray scattering structural studies were carried out at the Stanford Synchrotron Radiation Laboratory on the wiggler beamlines 6-2 and 10-2.
- H. E. Warriner, S. H. J. Idziak, C. R. Safinya, P. Pincus, in preparation.
- The interaction results from undulation-induced antidepletion forces (P. Pincus and C. R. Safinya in preparation).
- Samples were prepared in flat glass capillaries measuring 0.2 mm, 0.1 mm, and 0.05 mm thick, used as supplied by In Vitro Dynamics.
- S. A. Asher and P. S. Pershan, *Biophys. J.* **27**, 393

(1979); M. B. Schneider and W. W. Webb, *J. Phys. France* **45**, 273 (1984); P. Boltzenhagen, O. D. Lavrentovich, M. Kleman, *Phys. Rev. A* **46**, 1743 (1992).

26. On occasion, the gel mixtures contained a small amount of "spherulite"-type defects [that is, focal conic domains with positive Gaussian curvature (25); the "whispy" line defects that dominate have negative Gaussian curvature].

27. B. H. Cao and M. W. Kim, *Faraday Discuss.* **98**, 245 (1994).

28. U. Seiffert, *Phys. Rev. Lett.* **70**, 1335 (1993); T. Kawakatsu, D. Andelman, K. Kawasaki, T. Taniguchi, *J. Phys. II France* **3**, 971 (1993), and references therein.

29. W. Helfrich and W. Harbich, *Chem. Scr.* **25**, 2 (1985); also independently calculated by F. MacKintosh (private communication).

30. Z.-G. Wang and S. A. Safran, *J. Phys. France* **51**, 185 (1990).

31. K. Kawasaki and A. Onuki, *Phys. Rev. A* **42**, 3664 (1990).

32. F. Ilmain, T. Tanaka, E. Kokufuta, *Nature* **349**, 400 (1991); E. S. Matsu and T. Tanaka, *ibid.* **358**, 482 (1992); Y. Osada and S. B. Ross-Murphy, *Sci. Am.* **268**, 82 (May 1993); Z. Hu, X. Zhang, Y. Li, *Science* **269**, 525 (1995).

33. We are grateful to D. Lasic for many discussions regarding biomaterials based on poly(ethylene glycol)-lipid. We acknowledge useful discussions with J. Prost, T. Lubensky, D. Nelson, J.-B. Fournier, F. MacKintosh, and S. Safran. C.R.S. is especially grateful to P. Pincus for numerous extensive and instructive discussions on the physics of polymers at interfaces. P.D. acknowledges partial support from a NATO (North Atlantic Treaty Organization) research fellowship. Partially supported by National Science Foundation (NSF) (DMR-93-01199) and the Petroleum Research Fund (27837-AC7). The Materials Research Laboratory at Santa Barbara is supported by the NSF under grant DMR-9123048. The synchrotron experiments were carried out at the Stanford Synchrotron Radiation Laboratory, which is supported by the U.S. Department of Energy.

21 August 1995; accepted 27 November 1995

## Were Thick Galactic Disks Made by Levitation?

S. Sridhar\* and J. Touma

The thick disk of our galaxy displays kinematic and chemical properties that are intermediate between those of the halo and the (thin) disk stellar populations. Not all disk galaxies have a thick disk. A theory of the origins of a thick disk can potentially provide insights into the physical state of our galaxy in its infancy. Levitation, a process that relies on adiabatic capture into resonance of stellar orbits in a growing disk, is presented as a plausible formation mechanism; a 2:2 resonance between vertical and epicyclic oscillations drifts to large vertical energies as the disk grows adiabatically. Resonant stars levitate several kiloparsecs above the plane, forming a thick disk whose spatial distributions, kinematics, and ages leave unique observational signatures on the sky. The same process can also produce the disk globular cluster system.

In addition to the flat disks that give them their names, disk galaxies sometimes have a distribution of stars that forms a thick disk (1–5). Near the solar circle, the thick disk is a rapidly rotating population that extends to several kiloparsecs (kpc) above the galactic plane (6, 7). The processes that have heated the thin disk (8) cannot impart the large vertical velocities ( $>40 \text{ km s}^{-1}$ ) needed to support the thick disk (9). Several formation mechanisms have been proposed (10): some suggest that the thick disk formed during the dissipational collapse of our galaxy, whereas others propose the heating of a preexisting thin disk, for instance, by the accretion of a satellite galaxy. We present a dynamical model, levitation, whose essential ingredients are the slow growth of the disk plus largish initial eccentric motions of orbiting stars.

S. Sridhar, Canadian Institute for Theoretical Astrophysics, McLennan Laboratories, University of Toronto, 60 St. George Street, Toronto M5S 1A7, Canada, and Inter-University Centre for Astronomy and Astrophysics, Post Bag 4, Ganeshkhind, Pune 411 007, India.  
J. Touma, Canadian Institute for Theoretical Astrophysics, McLennan Laboratories, University of Toronto, 60 St. George Street, Toronto, M5S 1A7, Canada.

\*To whom correspondence should be addressed.

Gas falling into the potential well of a dark halo will settle into a disk if it can dissipate energy efficiently (11, 12). While stars form, more gas continues to be added to the disk. If the disk is axisymmetric, as we assume it is, the orbital angular momentum  $L$  of each star is conserved, which results in an inward drift of the guiding-center radii ( $R_0$ ) of all orbits. It is likely that the disk grows over times much longer than the orbital periods of stars (that are not too far out in the disk) (13, 14). In situations such as these, when the forces vary slowly and the dynamics is nearly integrable, it is useful to consider the actions associated with a stellar orbit;  $L$  is one such action. The other two are associated with the epicyclic and vertical oscillations about the inwardly drifting circular motions of the guiding center (15). If  $X = (R_{\text{max}} - R_0)$  is the amplitude of the radial oscillations,  $Z$  is the amplitude of the vertical oscillations, and  $U$  and  $W$  are the corresponding velocity amplitudes, then  $I_R = XU$  and  $I_z = ZW$  will suffice, for our purposes, as surrogates for the true radial and vertical actions. The normal response of a stellar orbit to the adiabatically growing disk potential will be to conserve  $I_R$

and  $I_z$  (15). Because the frequencies  $U/X$  and  $W/Z$  may be expected to increase with disk mass, spatial amplitudes decrease while velocities grow. In particular, the vertical thickness of the disk will decrease while the vertical velocity dispersion grows by a corresponding factor. When there are resonances between radial and vertical oscillations, the relative phase might be even more slowly varying than the disk potential, thus breaking adiabatic invariance (16). If an orbit happens to be captured into resonance (17–19), the star may be dragged across phase space along with the slowly drifting resonance, resulting in a change of order unity in the actions.

Levitation is a process that relies on just such a capture into resonance. We will describe this mechanism after introducing a specific form for the potential of the dark halo:

$$\phi_h = (V_c^2/2) \ln[R_c^2 + R^2 + (z/q)^2] \quad (1)$$

where  $R = \sqrt{x^2 + y^2}$  is the radius in the equatorial plane,  $z$  is the height above this plane,  $R_c$  is the core radius,  $1/\sqrt{2} < q < 1$  measures the flatness of the potential, and  $V_c$  is the characteristic circular speed due to halo potential. When the disk is still very light,  $\phi_h$  will essentially govern the motions of stars. The ratio of vertical to epicyclic frequency (for small  $X$  and  $Z$ ) is

$$\nu_h/\kappa_h = 1/q\sqrt{2} < 1 \quad (2)$$

The growing disk will add to both frequencies in quadrature;  $\nu^2 = \nu_h^2 + \nu_d^2$ , and  $\kappa^2 = \kappa_h^2 + \kappa_d^2$ . Because the disk is geometrically very flat, it will add more to  $\nu$  than to  $\kappa$ . At the present time, near the solar circle,  $\nu/\kappa \approx 3$ , so sometime in the remote past the frequencies must have been equal; that is, the star must have passed through resonance. An important property of both  $\nu$  and  $\kappa$  is that they are decreasing functions of  $X$  and  $Z$ . Thus, a star that came into resonance when  $\nu \approx \kappa$  can remain locked in resonance only by increasing both  $Z$  and  $W$ . A resonant star will rise far above the plane while its nonresonant fellows are crunched by the growing disk. This implies that the actions are no longer conserved quantities, and indeed they are not. What is conserved is the combination,  $(I_R + I_z)$ , so that levitation works by exchanging (an initially largish)  $I_R$  for (an initially smallish)  $I_z$ . The 2:2 resonance gets its name from the  $z^2(R - R_0)^2$  terms in the combined potential of the halo and the disk that are the dominant providers of confinement near the drifting resonance [see (19) for more details of the dynamics]. The strength of this nonlinearity as well as the slowness of growth of the disk determine how many stars are captured and how far in phase space they are dragged along by the resonance before they escape.